Measurements and Analysis of Electrostatic and Magnetic Fluctuations in TBR-1

Maria Vittoria A.P. Heller, Raul M. Castro, Iberê L. Caldas,
Zoezer A. Brasilio, Ruy P. da Silva, (TBR-1 Team)
Instituto de Física, Universidade de São Paulo
C.P. 20516, 01498-970 São Paulo, SP, Brazil

Received March 18, 1993; revised manuscript received June 4, 1993

In order to measure the mean and fluctuation parts of plasma parameters, various types of Langmuir and magnetic probes have been designed and installed in the edge region of TBR-1 tokamak. These probes are arranged as an array specially designed to measure, simultaneously, electrostatic and magnetic turbulence observed in this region, besides determining plasma density, potential, and temperature. Advanced digital signal analysis techniques, including a bispectral estimation method, were used to obtain spectra correlations, phase relationships, and degree of fluctuation coupling. Thus, it was possible to identify characteristics of the observed strong and high dispersive turbulence and to compute the connected electrostatic fluctuation induced particle transport.

I, Introduction

It is well known that large amplitude, broadband density and electrostatic potential fluctuations occur at the edge of tokamak plasmas[1,2]. These fluctuations are responsible for a significant portion of particle loss rate, and may account for a large part of the anomalous energy losses observed in magnetic confined plasmas[1].

A general and important feature of these fluctuations is the observed wide range of frequencies, at a given wave number, which supports the conclusion that the naturally occurring waves are described as a turbulence. In fact, the experimental investigation of these phenomena is very complex due to the simultaneous presence of many waves, possible nonlinear interactions between them, noise, and turbulence. This investigation has been partially done with probes, which play an important role in the characterization of plasma edge turbulence[3,4,5].

In order to study the mean and fluctuation parts of plasma parameters, a complex system of probes[6] was designed and installed in the TBR-1 tokamak. A distinguishing feature of these probes was to compose a diagnostic system specially designed to measure, simultaneously, and within a short distance (few millimeters), electrostatic and magnetic fluctuations, in addition to relevant plasma parameters, as density, potential, and temperature.

The acquired data were digitized, and submitted to a specific power spectral analysis to quantify several statistical properties of the turbulent fluctuations in the plasma edge. With these data, as a consequence of the performed numerical analysis, it was also possible to estimate the particle flux caused by these fluctuations. The particle flux values thus obtained were of the same order of magnitude as those directly computed from particle diffusion measurements. Furthermore, with this spectral analysis, an algorithm recently introduced[7] to verify nonlinear wave-wave coupling in fluctuations was also used, and no predominant coupling between any specific modes (a characteristic of weak turbulent plasmas) was identified.

In section II the experimental set-up is described; in section III, the spectral analysis techniques used in this work, such as cross-correlations, wave-number frequency spectra $S(k, f)$, and some tools to demonstrate the role of nonlinear wave coupling in the interaction processes, are presented. Section IV contains some results and discussions, and section V some conclusions, obtained with these signal processing techniques.

II. Experimental Set-up

The Tokamak TBR-1[8] is a small device in which the plasma is created inside a stainless steel vessel. Its main parameters are: major radius R = 0.30 m, poloidal plasma limiter radius a = 0.08 m, vessel radius b =

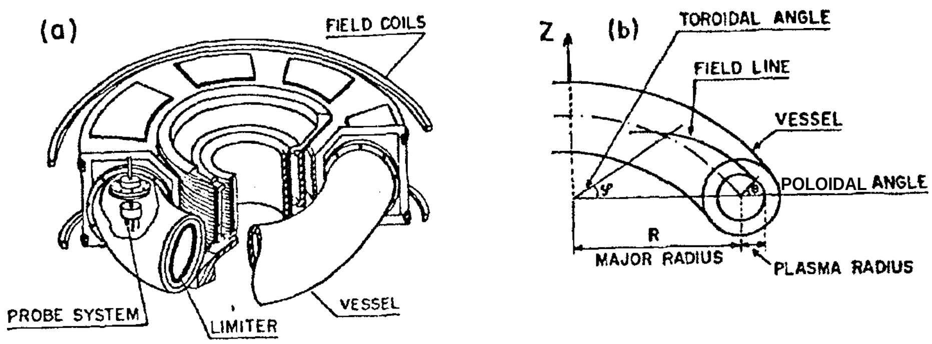

Figure 1: (a) Scheme of TBR-1 Tokamak. (b) Scheme of coordinate system.

0.11 m (Fig. 1a.b). The gas used in this experiment was hydrogen with a base pressure of 8.7×10^{-5} mbar. For the reported experiment, the machine was operated with a central electron temperature $T_e(0) \cong 2 \times 10^2$ eV, central density $n_0 \cong 6 \times 10^{18}$ m^{-3}, plasma current $Ip \cong$ 8.5 kA, toroidal field $B_\phi = 0.4\,T$, and loop voltage $V_\ell \leq$ 1.5 V (Fig. 2).

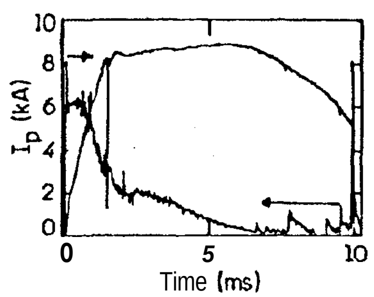

Figure 2: Time evolution of plasma current, Ip, and loop voltage V_ℓ for typical pulses of TBR-1.

The probe assembly is mounted on a port hole at the top of the tokamak, along the plasma centerline at 45° from the liiniter and on a structure that permit a radial movement in the vessel.

A scheme of the arrangement of the probes is shown in Fig. 3. The used Langmuir probe array has four tungsten wire tips of 2×10^{-3} m long, 5×10^{-4} m diameter, configured in 2×2 square matrix with 2×10^{-3} m spacing. Two of the probe tips are connected to measure floating potential fluctuations, ($\tilde{\varphi}$), and the other two connected to collect the ion saturation current to measure density fluctuations ($\tilde{n}$).

Other three tips of the same previously specified dimensions are biased as a triple probe[9,10]. The triple probe is used to measure the mean plasma density, n, electron temperature, T_e, and floating potential (Fig. 4). In this probe a constant voltage (50 V) is applied between two tips and the third probe potential (φ_f) is floating. T_e and n are determined from the probe current flowing through the biased two tips, and the potential difference between the positively biased tip and the third floating tip, $\varphi_+ - \varphi_f$. The temperature is given by:

$$T_e = \frac{1}{\ln 2}\,(\varphi_+ - \varphi_f) \quad . \tag{1}$$

The determination of density and plasma potential is obtained from the measurement of ion saturation current, I,,, and floating potential using the equations:

$$I_{s_i} = n\,e\,A\,f\left(\frac{T_i}{T_e}\right)\left[\frac{K(T_e+T_i)}{m_i}\right]^{1/2} \tag{2}$$

and

$$\varphi_p = \varphi_f - \left(\frac{kT_e}{2e}\right)\left\{\ln\left[\frac{2\pi m_e}{m_i}\left(1+\frac{T_i}{T_e}\right)\right]-1\right\} \quad , \tag{3}$$

where A is the tip area, K the Boltzmann constant, m_i the ion mass, T_e and T_i, respectively, the electron and the ion temperature, f is a function that depends of the model adopted[11], and φ_p is the plasma potential.

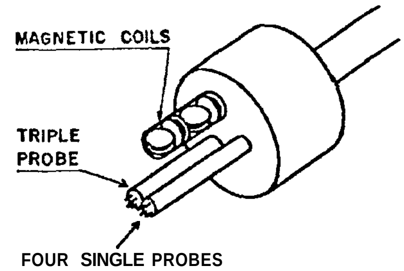

Figure 3: Probe head view.

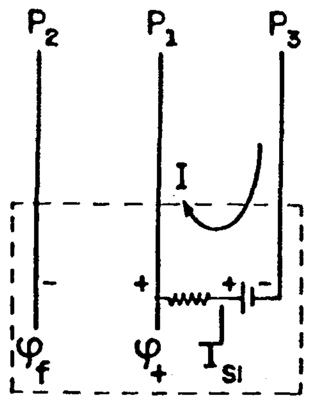

Figure 4: Scheme of triple probe.

Fig. 5 shows a diagram of the data acquisition probe system. The circuits used for the measurement of floating potential, and ion saturation current, have typically high input impedance and frequency response in the range 3–500 kHz. In the triple probe, the circuits for measurement of φ_+ and φ_f have high input impedance and response frequency with a 15 kHz cutoff. An isolation amplifier is used to measure the ion saturation current.

Four coils, two poloidally and two radially oriented, were mounted in the same system at 2.3×10^{-2} m from the Langmuir probes. As the voltage induced in the coils is proportional to the rate of change of magnetic flux, they provided radial profiles of poloidal and radial field component fluctuations (B_θ and B_r).These fields can be measured with a frequency response up to 500 kHz.

The probes signals are digitally recorded at a sampling frequency of 1 MHz to allow measurements up to the Nyquist frequency of 500 kHz. To avoid frequency aliasing, low pass filters have been used with cutoff frequencies lower than 300 kHz. All measured quantities are taken in the time interval of 2 ms during the current flat to~₃nd averaged over four consecutive shots. The length of the used data consists of 62 samples of 128 points. Measurements have been made in the region accessible to the probes, $r/a \cong 0.87$–1.25. In the present analysis the effect of temperature fluctuations on the computation of saturation current fluctuations in terms of density fluctuations is neglected. As an example, Fig. 6 shows temporal profiles of floating potential, ion saturation current, magnetic poloidal fluctuation and electron temperature at $r/a = 0.99$. All the three initial traces display a high level of fluctuations.

III. Spectral analysis and applications

The digital power spectra analysis applied in the next section[7,12] will now be introduced. The subsequently defined functions are computed from digitized time-varying signals, $x(t)$ and $y(t)$, obtained with the probes, and their Fast-Fourier-Transform (FFT), $X(f)$ and $Y(f)$.

a) *Cross correlation*

The cross-power spectrum $P_{xy}(\mathrm{f})$ can be expressed as:

$$P_{xy}(\mathrm{f}) = |P_{xy}(f)|\, e^{i\theta_{xy}(f)} \quad , \tag{4}$$

where $|P_{xy}(f)|$ is the cross-amplitude spectrum given by:

$$P_{xy}(f) = X^*(f)\,Y(f) \quad , \tag{5}$$

and $\theta_{xy}(f)$ is the phase spectrum given by:

$$\theta_{xy}(f) = \theta_y(f) - \theta_x(f) \quad , \tag{6}$$

the phase spectrum is a direct measure of the dispersive characteristics of the wave system i.e.,

$$\theta_{xy}(f) = \vec{k}(f) \cdot \Delta\vec{r} \quad , \tag{7}$$

were $\vec{k}$ is the wave vector and ***Ar'*** is the vector distance of separation of the points at which the fluctuations were monitored.

Although this and the subsequent definitions are valid for any $\vec{k}$ component, in this work, due to the chosen probe array, only the poloidal component, k_θ, was measured. Thus, $\vec{k}\cdot$ Ar'= $k_\theta \Delta\theta$.

Another function used in this work was the coherence spectrum, which is defined as follows:

$$|\gamma_{xy}(f)| = \frac{|P_{xy}(f)|}{[P_{xx}(f)\; P_{yy}(f)]^{1/2}} \quad . \tag{8}$$

The coherence spectrum measures the degree of mutual coherence between two signals, it is a real positive number lying in the interval $0 \le |\gamma_{xy}| \le 1$. In this work, the coherence spectrum is necessary to compute the particle plasma transport due to electrostatic fluctuations (Eq. 15).

b) The wavenumber-frequency *spectrum,* $S(k,\mathrm{f})$

A description of turbulence is provided by the wavenumber-frequency spectrum $S(k,\mathrm{f})$ [7,12] which describes the fluctuation power resolved as function of wavenumber and frequency.

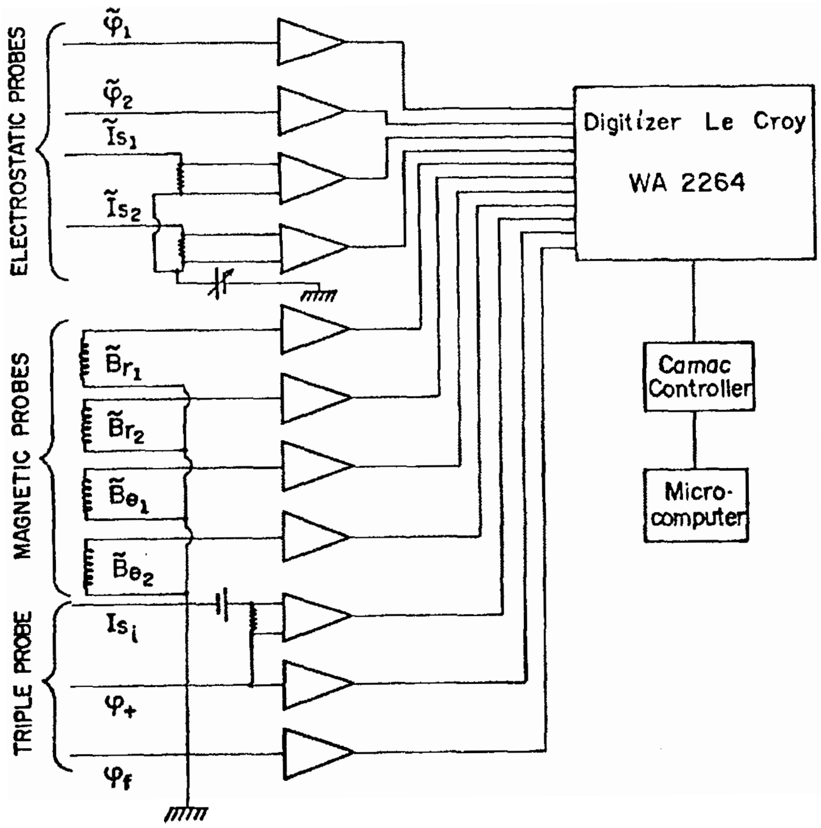

Figure 5: Diagram of probe the data acquisition system.

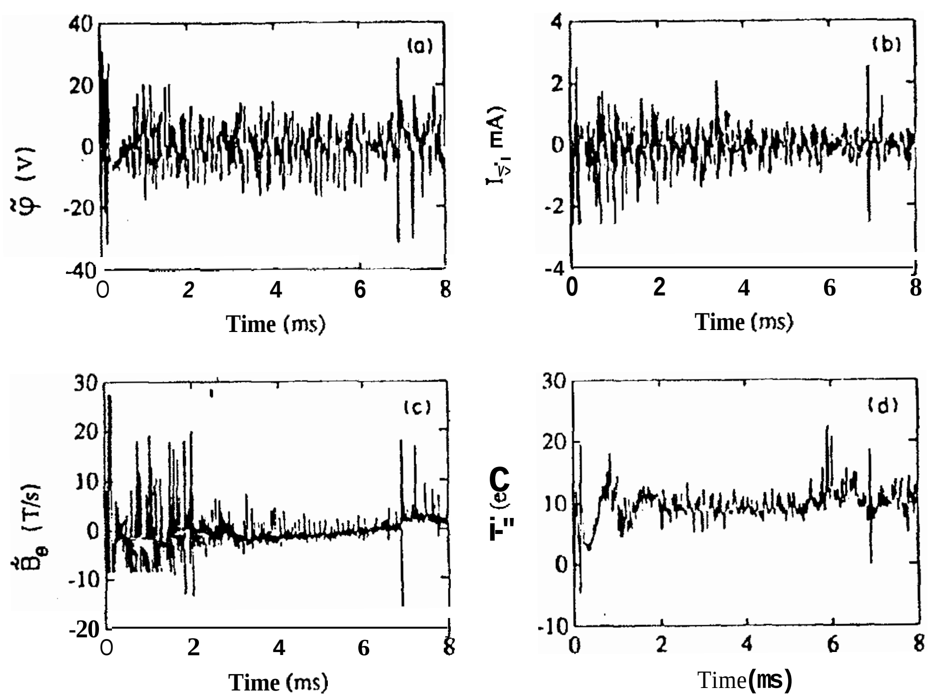

Figure 6: Temporal behaviour for potential fluctuations ($\tilde{\varphi}$), (a), and saturation current, I,,, (b), at $r/a = 0.99$; magnetic poloidal fluctuations, $\widetilde{B}_\theta$, (c), at $r/a = 1.26$; temporal profile of electron temperature, T_e, (d), at $r/a = 0.99$.

Thus, a statistical dispersion relation $\bar{k}(f)$ and its spectral width $\sigma_k(f)$ can be defined as

$$\bar{k}(f)=\sum_{k} k \frac{s(k,f)}{\sum_{k} s(k,f)} \quad ,s(k,f)=\frac{S(k,f)}{\sum_{k,f} S(k,f)}, \quad (9)$$

and

$$\sigma_k(f)=\left[\left\{\sum_{k}\left(k^2\frac{s(k,f)}{\sum_{k} s(k,f)}\right)-\bar{k}^2(f)\right\}\right]^{1/2}. \quad (10)$$

Analogous quantities may also be represented in terms of wavenumber.

In addition, it is possible to extract the apparent propagation velocity for the bulk of the turbulence which is given by

$$v_{ph}=\sum_{k,f}\left(\frac{2\pi f}{k}\right) s(k,f). \quad (11)$$

As $k=k_\theta$, this gives the phase velocity in the poloidal direction.

The adequate probe separation (to obtain good spatial resolution on the measurements of the wave vector k by the used two point technique) is determined by the ion Larmor radius, r_{L_i}, since the typical mean electrostatic wave vector is given by $\bar{k}\lesssim r_L^{-1}$, at the plasma edge[12].

c) Bispectrum

Linear spectrum analysis techniques are of limited value when various spectral components interact with one another due to nonlinear process. In such case, higher order spectral techniques[7,13] are necessary to characterize the fluctuating signal, since the nonlinearities result in new spectral components being formed, which are phase coherent. The detection of such phase coherence may be carried out with the aid of high order spectra. The digital bispectral analysis techniques permit to investigate nonlinear wave-wave interactions.

The bicoherence spectrum may be utilized to distinguish between spontaneously excited modes and coupled modes in a self-excited fluctuation spectrum. The discrimination is based on the fact that the bicoherence spectrum (Eq. 13) is capable of detecting the phase coherence which characterizes the coupled-mode case.

The auto-bispectrum $B_{xxx}(f_1,f_2)$ is defined as[7]

$$B_{xxx}(f_1,f_2)=\langle X(f_1)\,X(f_2)\,X^*(f_1+f_2)\rangle \quad . \quad (12)$$

If the waves present at f_1, f_2 and f_1+f_2 are spontaneously excited independent waves, each wave may be characterized by statistically independent random phase mixing effect. On the other hand , if the three spectral components are nonlinearly coupled to each other, the total phase of the three waves will not be random, although phases of each wave are randomly changing for each realization. Consequently, the statistical averaging will not lead to a zero value of the bispectrum.

The bicoherence spectrum is defined as:

$$b^2(f_1,f_2)=\frac{|B_{xxx}(f_1 f_2)|^2}{|X(f_1+f_2)|^2\,|X(f_1)\,X(f_2)|^2}. \quad (13)$$

The bicoherence $b^2(f_1,f_2)$ will take a value close to unity when the wave at $f=f_1+f_2$ is excited by the coupling of the waves at f_1 and f_2. The bicoherence also measures the fraction of power at f_1+f_2 due to the three-wave coupling.

d) Transport

The transport associated with a given spectral band depends not only on the phase angle but also on the degree of coherence between the density and potential fluctuations in the same band. Following Ref. 7 the particle flux is estimated directly from correlations in $\tilde{\varphi}$ (potential) and $\tilde{n}$ (density). The particle flux Γ results from $\langle\tilde{n}\tilde{v}\rangle$ convection out of the edge, where $\tilde{v}$ is the fluctuating radial velocity given by

$$\tilde{v}\approx\left|\frac{\tilde{\vec{E}}\times\vec{B}_\phi}{B_\phi^2}\right|\cong\frac{k_\theta\tilde{\varphi}}{B_\phi}, \quad (14)$$

where B_ϕ is the toroidal component of the magnetic field. The wavenumber k_θ is determined from the statistical dispersion relation for potential fluctuations, and the electrostatic approximation is assumed to be valid. The particle flux is given by

$$\begin{aligned}\Gamma &= \sum_f \Gamma(f),\\ \Gamma(f) &= \frac{1}{B_\phi}\sqrt{P_{\tilde{n}\tilde{n}}}\,\sqrt{P_{\tilde{\varphi}\tilde{\varphi}}}\;k_\theta(f)\,\gamma_{\tilde{n}\tilde{\varphi}}\,\mathrm{sen}\,\theta_{\tilde{n}\tilde{\varphi}}(f).\end{aligned} \quad (15)$$

The phase angle of the density, relative to the potential, $\theta_{n\varphi}$, is computed from the phase of the cross-power spectrum between $\tilde{n}$ and $\tilde{\varphi}$, and together with the sign of $k_\theta(f)$, it determines the direction of the particle flux (radially inward or outward). The quantity $\gamma_{n\varphi}(f)$ is the degree of mutual coherence between density and potential, included to account for the decorrelation of $\tilde{n}$ with $\tilde{\varphi}$ as a result of their turbulent nature.

IV. Results and Discussion

The spectral analysis described in the preceding section was used to determine, from the computer-generated power-spectra, the squared amplitude, frequency, wavcnumber, and coherence from each of the several waves simultaneously present in the plasma.edge of the TBR-1.

Fig. 7 shows the normalized rms fluctuating amplitudes for density and potential. Root-mean-square fluctuation levels are typical of those obtained in other small and medium tokamaks; $\tilde{n}/\langle n\rangle$ decreases toward the inner region and $e\tilde{\varphi}/KT_e$ has a maximum near the limiter[3,4,5,14].

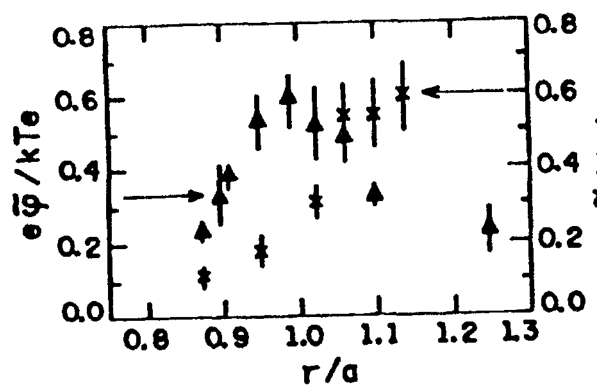

Figure 7: Radial dependence of the normalized rms fluctuating amplitudes for density ($\times$) the same for potential ($\blacktriangle$).

Fig. 8a shows the wavenumber frequency spectrum $S(k,\mathrm{f})$ at $r/a = 0.91$ for potential fluctuations (obtained,from two probes poloidally separated by 2 mm). Its shape appears broad and asymmetric about $k_\theta = 0$. The fluctuation power is confined to frequencies f $<$ 150 kHz and wavenumbers $|\ k_\theta\ | < 3.5 \times 10^2\ \mathrm{m}^{-1}$. Density fluctuations have similar spectra. The dispersive widths σ_k and σ_f were calculated and, in the edge plasma, had about the same value for density and potential spectra (typically $\sigma_k \cong 1 \times 10^2\ \mathrm{m}^{-1}$ and $\sigma_f \cong 1 \times 10^5$ Hz). The strength of the reported turbulence can be shown by the relative broadening $\sigma_{k_\theta}/k_\theta \cong 1.6$ (see Fig. 8b), higher than those obtained in similar experiments in other tokamaks for which the values of this ratio was about one[3,12,14].

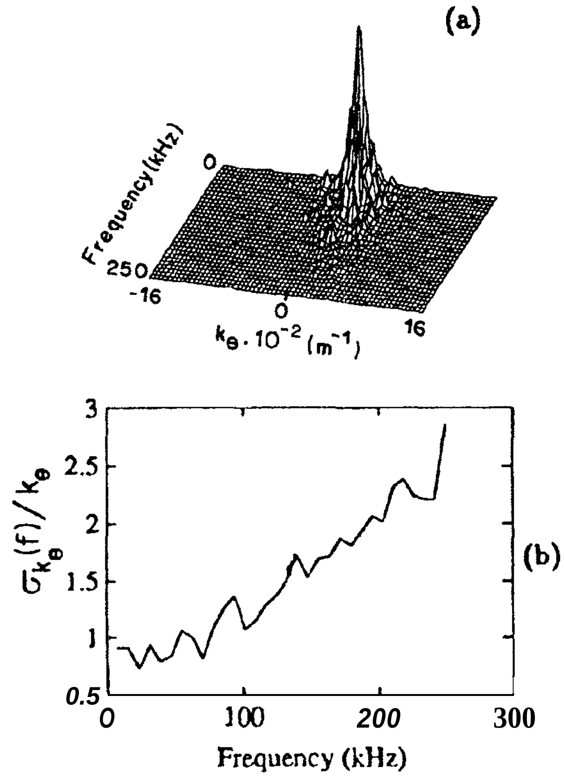

Figure 8: (a) $S(k_\theta,\mathrm{f})$ spectrum for potential fluctuations at $r/a = 0.91$. (b) Dispersion relation, $\sigma_{k_\theta/k_\theta}$ for the same position.

Power weighted poloidal phase velocities, obtained from Eq. 11 (in terms of k and $s(k,\mathrm{f})$),are of the same order of magnitude as the ion diamagnetic drift velocity, tipically $v_{ph} = 1 \times 10^3$ m/s; these velocities have also the same direction. Although no evidence of a shear layer was found (examining the v_{ph} and the $E_r \times B$ profiles) in the region accessible to the probes, there may exist a shear-layer (in a more internal region) displaced by the stochasticity enhancement[15].

The radial induced particle flux $\Gamma(f)$ due to electrostatic fluctuations was estimated from Eq. 15. Fig. 9a presents the particle flux spectra at to different radial positions; inside plasma and in the limiter shadow. This figure shows outward fluxes over the entire spectrum, but while inside the plasma a broad frequency spectrum is clearly observed, in the shadow of the limiter only a

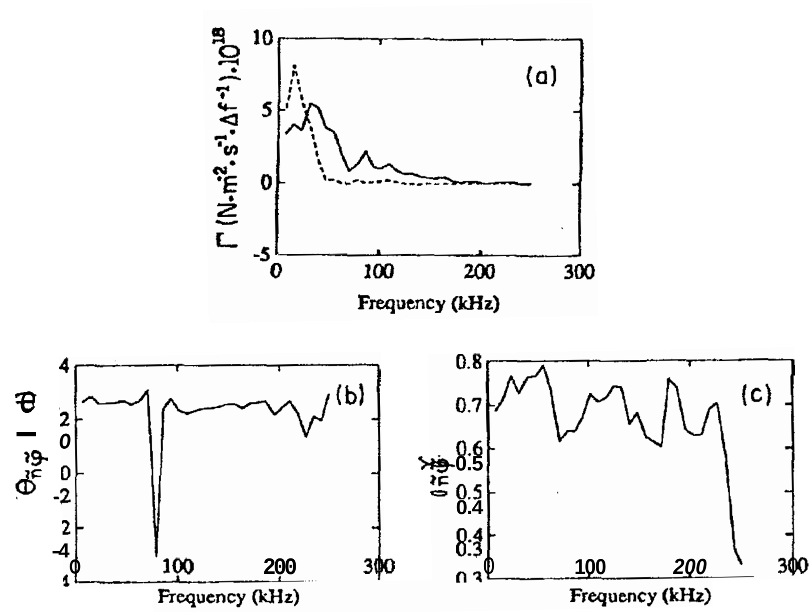

Figure 9: (a) Farticle flux spectra at $r/a = 0.95$ (—), and $r/a = 1.1$ (. ·) (Af = 7.8 kHz), (b) Phase spectrum of $\tilde{n}$ and $\tilde{\varphi}$ at $r/a = 0.95$, (c) Coherency spectrum of $\tilde{n}$ and $\tilde{\varphi}$ for the same position.

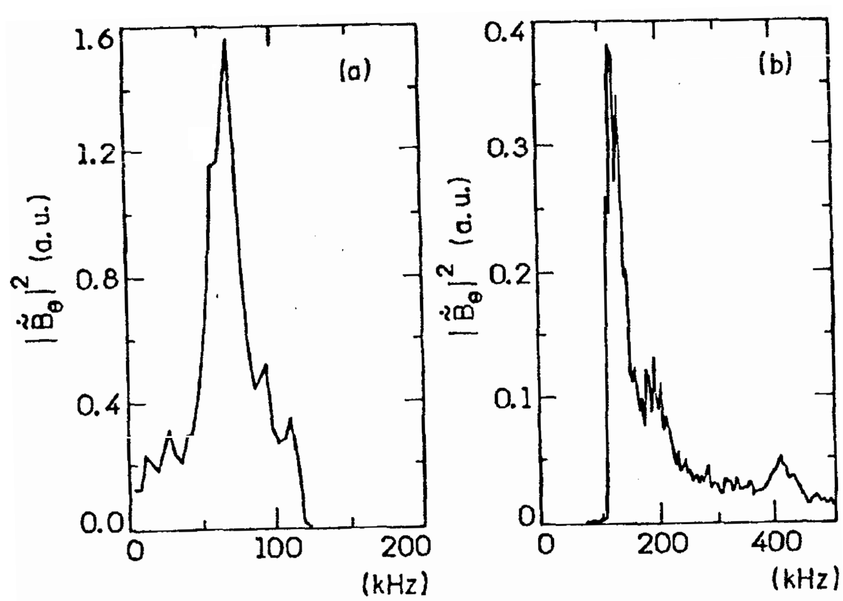

Figure 10: (a) Typical $\tilde{B}_\theta$ power spectrum in the coherent MHD frequency range, at $r/a = 1.16$. *(b)* Typical $\tilde{B}_\theta$ power spectrum in the broad band activity frequency range.

predominant low frequency peak can be identified. This contrast indicates the importance of inserting probes in tlie plasma edge to obtain information about its turbulence, i.e., its electrostatic broad-band spectrum. Furthermore, integrating $\Gamma(f)$, one obtains, for these fluctuation induced fluxes, values ($\Gamma \sim 1 \times 10^{19}$ particles $m^{-2}s^{-1}$) comparable to those computed directly from the anomalous particle diffusion[11]. From these values one can estimate diffusion coefficients ($D \sim 1\ m^2s^{-1}$) and confinement times ($\tau \sim 1 \times 10^{-3}$ s) compatible with other previous TBR-1 results[11].

Since $\Gamma(f)$ depends on the phase angle, $\theta_{\tilde{n}\tilde{\varphi}}$, and the coherence spectra, $\gamma_{\tilde{n}\tilde{\varphi}(f)}$, these are also shown in the Figs. 9b,c. From these figures, it is possible to recognize that $\sin\theta_{\tilde{n}\tilde{\varphi}}$ and $\gamma_{\tilde{n}\tilde{\varphi}}$ do not change much in the range $f < 150$ kHz. Therefore, the electrostatic frequency spectra are mainly determined by the $\tilde{n}$ and $\tilde{\varphi}$ amplitude dependence on f (one example of this variation can be seen in Fig. 8a). These qualitative features of the transport spectrum were also observed a.t other radial positions.

Signals from the radial and the poloidal components of the fluctuating magnetic field were measured with pick-up coils, whose dimensions allow the measurement of the wavenumbers up to 3×10^{-2} m. Thus, Fig. 10a shows a typical $\widetilde{B}_\theta$ power spectrum in the coherent MHD frequency range (identified in other experientes in the TBR-1[16,17] for picli-up coil at $r/a = 1.16$, and Fig. 10b shows the same $\widetilde{B}_\theta$ power spectrum in the broad band frequency range. This composition has been also observed in other tokamaks[18], but in different frequency ranges, specially the MHD oscillations, whose frequencies are — for bigger tokamaks — much lower than in TBR-I. Consequently, in the TBR-1, the magnetic and density fluctuation spectra are not so separated, as in other machines, a characteristic that may contribute to check correlations, not yet observed[19], between these oscillations. The spectral shapes of $\widetilde{B}_\theta$ and $\widetilde{B}_r$ are similar for different radial positions. Another particular observation was reported elsewhere[6], about small peaks in coherency spectrum $\gamma_{\tilde{n}\widetilde{B}_\theta}(f)$, concentrated in the MHD frequency range.

To quantify the strength of the wave-wave coupling in the plasma edge turbulence, the bispectral analysis was applied to tlie obtained data. As an example, Fig. 11 shows the bicoherence spectrum (Eq. 13) for the case of poloidal magnetic fluctuations, probe at $r/a = 1.16$; the low value of bicoherence implied tliat the system is turbulent in the frequency space and cannot be described in terms of few nonlinear coupled modes, possibly only spontaneously excited independent modes. This behaviour is similar for all oscillations analysed in this work.

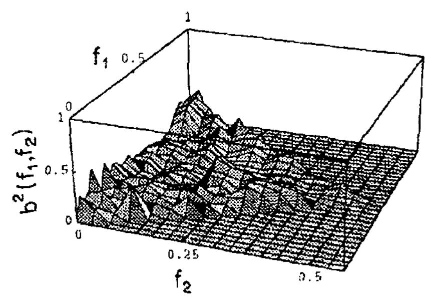

Figure 11: Bispectrum, $b^2(f_1, f_2)$, for poloidal magnetic field fluctuations at $r/a = 1.16$.

V. Conclusions

The application of spectral analysis to the fluctuation data obtained with the electric and rnagnetic probes installed in the TBR-1 were adequate to characterize the turbulence and mean parameter profiles at tlie plasma edge. Moreover, with the information obtained from these diagnostic techniques that includes power spectral analysis, it was possibie to determine the wavenumber frequency, the phase angle, the coherency, and the fluctuation induced transport spectra.

The electrostatic waves are highly dispersive, their spectra are broad, and asymmetric about $k_\theta = 0$; their power is confined to frequencies $f < 150$ kHz and wavenumbers $|k_\theta| < 3.5 \times 10^2\ m^{-1}$.

In TBR-1, as observed in other tokarnaks, the magnetic fluctuation frequency spectra can be interpreted as a superposition of a low frequency Mirnov (MHD) oscillations and high frequency turbulence. However, there were observed Mirnov oscillations with frequencies up to 80 kHz, higher than in other larger tokamaks. Consequently, there was a partial superposition between the MHD and the electrostatic spectra, an unusual characteristic of plasma edge fluctuations. Moreover, this MHD activity is higher than those usually observed in other tokamaks and creates a stochastic magnetic field in the plasma edge, which affects the plasma confinement[17,20].

The application of the bispectral analysis to data of the TBR-1 plasma edge indicated no evidence of any dominant coupling modes.

With the results presented in this work it was possihle to improve previous work[17,21] on turbulence at TBR-1 plasma edge.

Acknowledgments

The authors would like to thank Dr. Roger D. Bengtson, Dr. Hong Lin, and Dr. Steve McCool (Fusion Research Center, The University of Texas at Austin) for useful discussions during the development of this work.

References

1. D. C. Robinson, Proc. Int. Workshop on Small Scale Turbulence and Ariomalous Transport in Magnetized Plasmas (Cargèse 1986), Éditions de Physique, 21 (1986).
2. Ch. Hol enstein, R. Keller, A. Pochelon, F. Ryter, M. L. Sawley, W. Simm and H. Weisen, Proc. Int. Workshcp on Small Scale Turbulence and Anomalous Transport in Magnetized Plasmas (Cargèse 1986), Éditions de Physique, 181 (1986).
3. S. J. Levinson, J. M. Beall, E. J. Powers, R. D. Bengtson, Nuclear Fusion 24, 527 (1984).
4. Ch. P. Ritz, R. D. Bengtson, S. J. Levinson and E. J. Powers, Phys. Fluids 27, 2956 (1984).
5. Y. J. Kini, K. W. Gentle, Ch. P. Ritz, T. L. Rhodes and R. C. Bengtson, Phys. Fluids **B3**, 674 (1991).
6. R. M. Csstro, M. V. A. P. Heller, I. L. Caldas, R. P. da Silva, Z. A. Brasilio and TBR-1 Team, "Transport in the Plasma Edge of a Tokamak with High MHD Activity", Il Nuovo Cimento, in press (1993).
7. E. J. Powers, "Polyspectral Analysis and its Applications", The University of Texas at Austin (1990), to be published.
8. I. C. Nasiimento, A. N. Fagundes, R. P. da Silva, R. M. O. Galvão, E. Del Bosco, J. H. Vuolo, E. K. Sanada and R. Dallaqua, Proceedings of the Spring College on Fusion Energy (Trieste, 1980) ICTP-IAEA, 45 (1981).
9. S. L. Chen and T. Sekiguchi, J. Appl. Phys. 36, 2363 (1965).
10. H. Ji, H. Toyaina, K. Tamagishi, S. Shinohara, A. Fujisawa and K. Miyamoto, Rev. Sci. Instrum. 62, 10 (1991).
11. R. P. da Silva, Ph.D. Thesis, IFUSP, University of São Paulo (1989).
12. J. M. Beall, Y. C. Kim and E. J. Powers, J. Appl. Phys. 53, 3933 (1982).
13. Ch. P. Ritz, E. J. Powers and R. D. Bengtson, Pliys. Fluids **B1**, 153 (1989).
14. C. Hidalgo, J. H. Harris, T. Uckan, J. D. Bell, B. A. Carreras, J. L. Dunlop, G. R. Dyer, Ch. P. Ritz, A. J. Wootton, M. A. Meier, T. L. Rhodes and K. Carter, Nuclear Fusion 31, 1471 (1991).
15. H. Lin, Ph. D. Thesis, The University of Texas at Austin, Report FRCR#401 (1991).
16. A. Vannucci, 1. C. Nascimento and I. L. Caldas, Plasma Phys. Contr. Fusion **31**, 147 (1989).
17. I. H. Tan, I. L. Caldas, I. C. Nascimento, R. P. da Silva, E. Sanada and R. Bruha, IEEE Trans. Plasma Science PS-14, 279 (1986).
18. P. Mantica, G. Vayakis, J. Hugill, S. Cirant, R. A. Pitts and G. F. Matthews, Nuclear Fusion 31, 1649 (1991).
19. A. J. Wootton, The University of Texas at Austin, Report FRCR#371 (1990).
20. I. L. Caldas, M. V. A. P. Heller, M. Baptista, K. Ullinan, R. M. Castro, Z. Brasilio, R. P. da Silva and R. L. Viana, V LAWPP (México, 1992), invited paper, to be published.
21. A.N. Fagundes, D.F. Cruz Jr., R.M.O. Galvão, J.E. Irahuru, I.C. Nascimento, W. Sá, R.P. da Silva, A.G. Tuszel and A. Vannucci, Proc. Energy Independence Conference/Fusion Energy and Plasma Physics (Rio de Janeiro, 1987), World Scientific, 13 (1988).